Petroleum Science 22 (2025) 178–192

Contents lists available at ScienceDirect

Petroleum Science

journal homepage: www.keaipublishing.com/en/journals/petroleum-science

Original Paper

Internal-multiple-elimination with application to migration using two-way wave equation depth-extrapolation scheme

Jia-Chun You [a, *], Gu-Lan Zhang [b], Xing-Guo Huang [c], Xiang-Wen Li [d], Jun-Xing Cao [a]

[a] College of Geophysics, Chengdu University of Technology, Chengdu, 610059, Sichuan, China
[b] School of Geoscience and Technology, Southwest Petroleum University, Chengdu, 610500, Sichuan, China
[c] College of Instrumentation and Electrical Engineering, Jilin University, Changchun, 130021, Sichuan, China
[d] Bureau of Geophysical Prospecting Inc., China National Petroleum Corporation, Zhuozhou, 072751, Hebei, China

ARTICLE INFO

Article history:
Received 9 April 2024
Received in revised form
7 June 2024
Accepted 27 June 2024
Available online 28 June 2024

Edited by Meng-Jiao Zhou

Keywords:
Internal multiple elimination
Two-way wave equation depth-extrapolation scheme
Up/down wavefield separation
Migration

ABSTRACT

Internal multiple interference, affecting both seismic data processing and interpretation, has been observed for long time. Although great progress has been achieved in developing a variety of internal-multiple-elimination (IME) methods, how to increase accuracy and reduce cost of IME still poses a significant challenge. A new method is proposed to effectively and efficiently eliminate internal multiples, along with its application in internal-multiple-eliminated-migration (IMEM), addressing this issue. This method stems from two-way wave equation depth-extrapolation scheme and associated up/down wavefield separation, which can accomplish depth-extrapolation of both up-going and down-going wavefields simultaneously, and complete internal-multiple-elimination processing, adaptively and efficiently. The proposed method has several features: (1) input data is same as that for conventional migration: source signature (used for migration only), macro velocity model, and receiver data, without additional requirements for source/receiver sampling; (2) method is efficient, without need of iterative calculations (which are typically needed for most of IME algorithms); and (3) method is cost effective: IME is completed in the same depth-extrapolation scheme of IMEM, without need of a separate processing and additional cost. Several synthesized data models are used to test the proposed method: one-dimensional model, horizontal layered model, multi-layer model with one curved layer, and SEG/EAGE Salt model. Additionally, we perform a sensitivity analysis of velocity using smoothed models. This analysis reveals that although the accuracy of velocity measurements impacts our proposed method, it significantly reduces internal multiple false imaging compared to traditional RTM techniques. When applied to actual seismic data from a carbonate reservoir zone, our method demonstrates superior clarity in imaging results, even in the presence of high-velocity carbonate formations, outperforming conventional migration methods in deep strata.

1. Introduction

Internal multiples are commonly considered as an interference in seismic exploration. Because of strong energy, and small differences in traveling velocity compared to primary waves, internal multiples make significant interference to both seismic data processing (such as velocity analysis and imaging), and seismic data interpretation. Therefore, it is widely recognized that, it is necessary to perform internal multiple elimination before imaging (Yilmaz, 2001; Li and Qu, 2022).

However, eliminating internal multiples has historically been a challenging task in seismic data processing. Especially, how to increase accuracy and reduce cost of internal-multiple-elimination methods is still an active research topic today. To address this problem, numerous amounts of research works have been conducted, and a variety of different methods have been developed, during past decades. Many important works and articles on this hot topic are excellently summarized by Weglein and Dragoset (2005) in SEG Reprint, Matson and Dragoset (2005), Valenciano and Chemingui (2015) in Leading Edge, and Zhang et al. (2021) in Geophysics.

* Corresponding author.
E-mail address: youjiachun2009@163.com (J.-C. You).

https://doi.org/10.1016/j.petsci.2024.06.021

In general, four kinds of approaches for eliminating internal multiples have been developed in the past few years. The first kind of approach was proposed by Jakubowicz (1998), which, in principle, is an extension of surface-related-multiple-elimination (SRME; Verschuur et al., 1992) and applies both multidimensional convolution and cross-correlations on reflection data acquired at the measurement surface. The method does not necessitate prior information of velocity, and can effectively repress internal multiples in well-layered scenarios. Herrmann et al. (2008) further developed it and proposed a data-adaptive method to solve the amplitude error problem in predicted multiples, which vary smoothly based on location, frequency band, and angle. The second kind of approach is the common-focus-point (CFP) method. Berkhout and Verschuur (2005) broadened the Surface-Related-Multiple-Elimination method to internal multiple elimination, and introduced the CFP approach. Building upon this, Ikelle (2006) and Ikelle et al. (2009) introduced the concept of virtual seismic events, and applied it to prediction and suppression of internal multiples in synthetic data. Liu et al. (2013) proposed a new method for the propagation of seismic waves (with virtual reflection and virtual event), so that both forward and backward propagated waves, through convolution with significant waves, can be used to predict internal multiples. Qu et al. (2020) investigated the impacts of *Q*-attenuation and multiples in deep-marine environments and improved the quality and resolution of seismic imaging. Qu et al. (2021) proposes a viscoacoustic RTM method for different-order multiples to improve deep-sea seismic imaging by compensating for attenuation and utilizing multiples to enhance resolution and suppress artifacts. Chen et al. (2018) proposed a method to attenuate multiples in poststack seismic data through the approximation of conventional virtual events. In contrast to the traditional virtual event technique, the method introduced does not necessitate data regularization and provides greater computational efficiency, though it demands travel time information for primary waves. The third kind of approach involves the inverse scattering series (ISS) theory and its implementation in seismic data, as suggested by Weglein et al. (1997). The related methods are derived from the scattering theory and provide a multidimensional direct-inversion approach for suppressing internal multiples by identifying specific subseries. While it offers high accuracy, it comes with significant computational costs. Araújo et al. (1994), Coates and Weglein (1996), Weglein et al. (2003), and Malcolm and de Hoop (2004) applied the ISS method for internal multiple suppression under various challenging scenarios. Li and Hu (2009) suggested a methodology using the inverse scattering series based on the wave equation and Born series, where internal multiples are forecasted and eliminated through the creation of a subseries for surface-related multiples. This approach requires no information about the subsurface and is adaptable to various types of complex structures. Behura et al. (2014) achieved internal multiple elimination and artifacts-free imaging, founded on the inverse scattering theory. Löer et al. (2016) proposed an internal-multiple-elimination approach, based on inverse scattering series, which can provide one-step approximate prediction for all orders of internal multiples without need of model information. The fourth kind of approach is Marchenko scheme based, which was introduced to seismic application by Broggini et al. (2012, 2014), and Wapenaar et al. (2014). The core of this theory and method consists of two coupled equations called Marchenko equations, which are solved through iteration to obtain the so-called focusing functions (Neut et al., 2015; Meles et al., 2015). These focusing functions have the capability to concentrate at any specified imaging location in the subsurface, functioning as virtual sources or receivers responsible for generating or recording Green's functions (Behura et al., 2014; Slob et al., 2014). Meles et al. (2016) proposed an approximate approach to obtain primary reflections based on Marchenko theory, combined with reference-surface repositioning and convolutional interference. Thorbecke et al. (2017) and Jia et al. (2018) discussed the implementation of Marchenko method for calculating underground-to-surface Green's functions based on reflection measurements at the free surface and the earth surface respectively. A main advantage of this kind of approach is that related methods only require information of refection response data at the measurement surface, and direct-wave arrival time from the surface to imaging points. Because of this and other advantages, Marchenko method has been widely investigated and applied in different seismic applications and geological scenarios (Staring et al., 2016; Ravasi et al., 2016; Slob and Wapenaar, 2017; Lomas and Curtis, 2020; Zhang and Slob, 2020). Gu and Wu (2021) and Gu et al. (2023) retrieved primary reflections in the data domain using the Gel'fand-Levitan-Marchenko equation. Nevertheless, similar to the ISS approach, this kind of approach, in general, needs a sophisticated iterative scheme, and comes with a significant computational cost.

As we can see, a common feature for methods developed in the field of internal-multiple-elimination (IME) and internal-multiple-eliminated-migratio (IMEM), is that significant computational efforts are required, and typically such efforts are related to some iterative and sophisticated algorithms. In this document, we propose a different strategy and approach for IME and its application in IMEM. This method relies on two-way wave equation depth-extrapolation scheme (You and Cao, 2020; You et al., 2022) which can complete depth-extrapolation of up-going and down-going wavefields simultaneously and separate them from their two-way counterparts efficiently, at each depth-extrapolation step. It is proved that two-way depth-extrapolation scheme, combined with suitable boundary conditions and associated up/down wavefield separation, can remove internal multiples adaptively and efficiently at each depth-extrapolation step, in a much simpler way, via simultaneous depth-extrapolation of both up-going and down-going waves. Taking advantage of this, we develop and achieve a new internal-multiple-elimination and internal-multiple-eliminated-migration method, with following features: using same input data as that of conventional migration (source signature – for migration use only, macro velocity model, and receiver data), without need of additional requirements for source/receiver sampling; and being highly efficient method, completing IME directly without need of iterative calculations, and simultaneous IME and IMEM in the same depth-extrapolation scheme.

Our manuscript is organized as follows: first, we describe two-way wave equation depth-extrapolation scheme (with related boundary conditions and up/down wavefield separation) used in our proposed method; then, we describe theory of our proposed internal-multiple-elimination, and internal-multiple-eliminated-migration method, using two-way depth extrapolation scheme; next, we conduct numerical tests on several synthetic models and real data application to verify the effectiveness and accuracy of the proposed method in internal-multiple-elimination, and illustrate the performance and efficiency of the method in internal-multiple-eliminated migration; finally, we conclude with conclusions.

2. Theory

2.1. Two-way depth wavefield extrapolation scheme

2.1.1. Review of classic two-way propagator matrix

Two-way wave equation based wavefield-depth-extrapolation scheme, in space-frequency domain, reads (e.g. Kosloff and Baysal, 1983):

$$\frac{\mathrm{d}}{\mathrm{d}z}\mathbf{P}(\mathbf{x};\omega)=\mathbf{A}\mathbf{P}(\mathbf{x}_{\mathrm{R}};\omega), \tag{1}$$

where $\mathbf{P}(\mathbf{x};\omega)=\begin{bmatrix}p(\mathbf{x};\omega)\\ p_z(\mathbf{x};\omega)\end{bmatrix}$, $\mathbf{A}=\begin{bmatrix}0 & \mathbf{I}\\ L & 0\end{bmatrix}$, $L=-\frac{\partial^2}{\partial x^2}-\frac{\partial^2}{\partial y^2}-\frac{\omega^2}{v^2(\mathbf{x})}$, $\mathbf{I}$ is an identity matrix. $p(\mathbf{x};\omega)$ and $p_z(\mathbf{x};\omega)$ are pressure and divertive wavefield in the frequency domain, respectively; $\mathbf{x}=(x,y,z)=(\mathbf{x}_{\mathrm{H}},z)$ is space coordinates, defined in the Cartesian coordinate system, while $\mathbf{x}_{\mathrm{H}}=(x,y)$, is space coordinates in horizontal directions. $\mathbf{x}_{\mathrm{R}}$ represents the measured surface, and $\mathbf{x}$ the depth-extrapolated surface; $\mathbf{x}$ and $\mathbf{x}_{\mathrm{R}}$ have the same $\mathbf{x}_{\mathrm{H}}(x,y)$ but different vertical coordinates: z_{R} and z_x; the difference in vertical coordinates, between $\mathbf{x}$ and $\mathbf{x}_{\mathrm{R}}$, is defined as $\Delta z=z_x-z_{\mathrm{R}}$.

The solution of Eq. (1) can be expressed in form of propagator matrix (e.g. You et al., 2022):

$$\mathbf{P}(\mathbf{x};\omega)=\mathbf{W}\mathbf{P}(\mathbf{x}_{\mathrm{R}};\omega), \tag{2}$$

where $\mathbf{W}$ is a propagator matrix, $\mathbf{W}=\begin{bmatrix}W_{11} & W_{12}\\ W_{21} & W_{22}\end{bmatrix}$, $W_{11}=W_{22}=\cos(k_z\Delta z)$, $W_{12}=\sin(k_z\Delta z)/k_z$, $W_{21}=-k_z\sin(k_z\Delta z)$, and $k_z=\sqrt{\frac{\partial^2}{\partial x^2}+\frac{\partial^2}{\partial y^2}+\frac{\omega^2}{v^2(\mathbf{x})}}$. Note that k_z defined here is a symbolic notation which, in numerical practice, can be calculated in either space-frequency domain or wavenumber-frequency domain. In this paper, all mathematical equations and functions are expressions in space-frequency domain.

The differences between the two-way wave equation-based depth extrapolation scheme and the RTM algorithm are mainly embodied in two aspects: (1) Memory cost of wavefield calculation: the wavefield extrapolation implementation of RTM focuses on the time domain within the time slices, frequently requiring the storage of a huge wavefield matrix, e.g., $x\times y\times z\times tn$ for three-dimensional cases (x, y and z present sizes of velocity model, tn denotes the time samples); whereas the two-way wave equation based depth extrapolation scheme implements the wavefield extrapolation in the depth domain within the depth slices, which requires storing a relatively smaller wavefield matrix, e.g., $x\times y\times tn$ for three-dimensional cases, reducing a storage dimension saves a significant amount of storage space for wavefield computation. (2) Wavefield propagation differences: as for the incident wavefield, the reflection and transmission wavefields are generated on the both sides of the interface using the RTM method while the up-going wavefield (mirror image of the reflection wavefield) and the down-going wavefield (transmission wavefield), as shown in Fig. 1. Their differences in wavefield extrapolation implementation determine the potential application of the two-way wave equation based depth extrapolation scheme in internal multiples elimination.

2.1.2. Efficient up/down wavefield separation

To achieve an efficient separation of up-going and down-going wavefields, at each depth depth-extrapolation step, the above classic two-way wave equation wavefield depth-extrapolation scheme is reformulated as (You et al., 2022)

$$\widehat{\mathbf{P}}(\mathbf{x};\omega)=\widehat{\mathbf{W}}\widehat{\mathbf{P}}(\mathbf{x}_{\mathrm{R}};\omega), \tag{3}$$

where $\widehat{\mathbf{P}}(\mathbf{x};\omega)=\begin{bmatrix}p(\mathbf{x};\omega)\\ q(\mathbf{x};\omega)\end{bmatrix}$, and $\widehat{\mathbf{W}}$ is a reformulated propagator matrix, $\widehat{\mathbf{W}}=\begin{bmatrix}\widehat{W}_{11} & \widehat{W}_{12}\\ \widehat{W}_{21} & \widehat{W}_{22}\end{bmatrix}$, $\widehat{W}_{11}=\widehat{W}_{22}=\cos(k_z\Delta z)$, $\widehat{W}_{12}=\widehat{W}_{21}=i\sin(k_z\Delta z)$, and a new pressure wavefield, $q(\mathbf{x};\omega)$, is introduced and defined as

$$q(\mathbf{x};\omega)=p_z(\mathbf{x};\omega)/ik_z. \tag{4}$$

It is proved that, using the new pressure wavefield $q(\mathbf{x};\omega)$, decomposition of two-way wavefields to their one-way counterparts (up-going and down-going wavefields), can be efficiently completed at each depth depth-extrapolation step, via a simple summation operation. It is worth pointing out that one-way propagators, $\mathrm{e}^{ik_z\Delta z}$ and $\mathrm{e}^{-ik_z\Delta z}$, expressed in above reformulated depth-extrapolation scheme, are a simple summation of elements of two-way propagator-matrix (as defined in Eq. (3)):

$$\begin{cases}\widehat{W}_{11}+\widehat{W}_{12}=\mathrm{e}^{ik_z\Delta z}\\ \widehat{W}_{11}-\widehat{W}_{12}=\mathrm{e}^{-ik_z\Delta z}\end{cases}. \tag{5}$$

The relation between focusing functions (one-way propagators) and two-way propagator matrix, and its potential seismic applications are discussed in detail by Wapenaar et al. (2021) and Wapenaar and de Ridder (2022) recently. Eq. (5) verifies this relation, with a simpler form.

2.1.3. Boundary conditions and related two-way wave equation depth-extrapolation

In conventional seismic data acquisition, both the pressure wavefields and its vertical derivative, $p(\mathbf{x}_{\mathrm{R}};\omega)$ and $p_z(\mathbf{x}_{\mathrm{R}};\omega)$ are typically acquired or estimated, being known quantities. In this study, however, only up-going wavefield, $p_{\mathrm{u}}(\mathbf{x}_{\mathrm{R}};\omega)$, at the

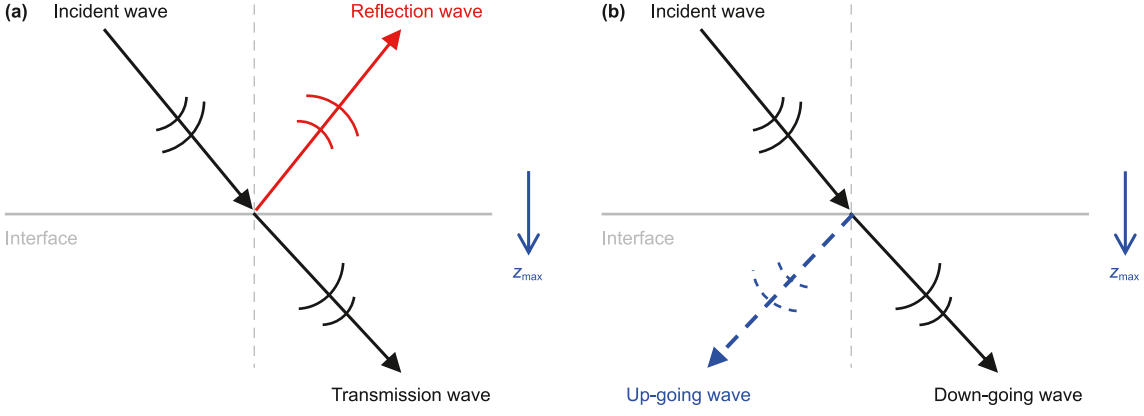

Fig. 1. Wavefield propagation by using **(a)** RTM and **(b)** two-way wave equation based depth extrapolation scheme.

measurement surface is used as input data (with surface-related-processing processed), which is equivalent to applying following boundary conditions: $p(\mathbf{x}_R;\omega) = p_u(\mathbf{x}_R;\omega)$, and

$$p_z(\mathbf{x}_R;\omega) = 0. \tag{6}$$

Inserting above boundary conditions (Eq. (6)) into the two-way propagator matrix (Eq. (2)), and using Eq. (4) to change $p_z(\mathbf{x};\omega)$ to $q(\mathbf{x};\omega)$, we can express $p(\mathbf{x};\omega)$ and $q(\mathbf{x};\omega)$ as follows:

$$\begin{cases} p(\mathbf{x};\omega) = \cos(k_z\Delta z)p_u(\mathbf{x}_R;\omega) = \dfrac{1}{2}\left(e^{ik_z\Delta z} + e^{-ik_z\Delta z}\right)p_u(\mathbf{x}_R;\omega) \\ q(\mathbf{x};\omega) = i\sin(k_z\Delta z)p_u(\mathbf{x}_R;\omega) = \dfrac{1}{2}\left(e^{ik_z\Delta z} - e^{-ik_z\Delta z}\right)p_u(\mathbf{x}_R;\omega) \end{cases}. \tag{7}$$

Based on Eq. (7), up/down decomposition of depth-extrapolated wavefields can be realized by summation operations:

$$\begin{cases} p_d(\mathbf{x};\omega) = p(\mathbf{x};\omega) + q(\mathbf{x};\omega) = e^{ik_z\Delta z}p_u(\mathbf{x}_R;\omega) \\ p_u(\mathbf{x};\omega) = p(\mathbf{x};\omega) - q(\mathbf{x};\omega) = e^{-ik_z\Delta z}p_u(\mathbf{x}_R;\omega) \end{cases}, \tag{8}$$

where $p_u(\mathbf{x};\omega)$ and $p_d(\mathbf{x};\omega)$ are respective up-going and down-going waves, at surface $\mathbf{x}$, after two-way depth-extrapolation and up/down wavefield separation.

It is worth emphasizing that although only up-going waves are existed in input data (Eq. (6)), both up-going and down-going waves are generated and propagated (as described by Eq. (7)), using two-way wave equation depth-extrapolation scheme. In addition, with reformulated two-way depth extrapolation scheme (Eq. (3)), up-going and down-going waves can be separated and obtained efficiently from their two-way counterparts, via a summation operation at each depth step (as indicated by Eq. (8)). In remaining text of this paper, above features of two-way depth-extrapolation scheme and associated up/down wavefield separation scheme are further explored and used for developing a new method of internal-multiple-elimination, and related multiple-eliminated-migration.

2.2. Internal-multiple-elimination using two-way depth-extrapolation scheme

2.2.1. Internal multiple generators

For horizontally layered media, internal-multiples are sorts of multiple reflections generated by "two-interfaces" and combinations of such "two-interfaces", as schematically shown in Fig. 2. In this paper, we call each interface of such "two-interfaces" as "multiple-generator" or simply "generator". With this definition of multiple-generator, multiples caused by any two subsurface generators, are called internal-multiples; space coordinates of any $n+1$ generators can be defined as $\mathbf{x}_j$ ($j = 0, 1, 2, \ldots, n$), with corresponding depths:

$$z_j = l_j dz - z_R, \tag{9}$$

where l_j (j = 0, 1, 2, …, n) are arbitrary numbers (from small to large), smaller than N (the largest depth steps in extrapolation); dz denotes depth-step interval; and z_R is vertical coordinate of $\mathbf{x}_R$ (same as defined in Eq. (2)). With above definition of generators, for any j-th generator ($j > 0$), we have j generator-pairs consisting of the j-th generator and corresponding shallower generators: (x_0, x_j); (x_1, x_j); …; and (x_{j-1}, x_j). Under this assumption of multiple-generator, in following, we describe how the proposed method can realize adaptive internal-multiple-elimination in two-way depth-extrapolation scheme, and what are main features of our proposed method.

2.2.2. Adaptive internal-multiple-elimination without need of source wavelet and iterative prediction

Input receiver data recorded at the measurement surface $\mathbf{x}_R$, $p_u(\mathbf{x}_R;\omega)$, can be expressed as follows:

$$p_u(\mathbf{x}_R;\omega) = p_0(\mathbf{x}_R;\omega) + \mathrm{IM}(\mathbf{x}_R;\omega), \tag{10}$$

where $p_0(\mathbf{x}_R;\omega)$ and $\mathrm{IM}(\mathbf{x}_R;\omega)$ are primary waves and multiples, respectively. If there are $n+1$ subsurface multiple generators (as defined in Eq. (9)), $p_0(\mathbf{x}_R;\omega)$ and $\mathrm{IM}(\mathbf{x}_R;\omega)$ can be expressed as

$$p_0(\mathbf{x}_R;\omega) = p_0^1(\mathbf{x}_R;\omega) + p_0^2(\mathbf{x}_R;\omega) + \cdots + p_0^n(\mathbf{x}_R;\omega) = \sum_{j=1}^{n} p_0^j(\mathbf{x}_R;\omega) \tag{11}$$

$$\mathrm{IM}(\mathbf{x}_R;\omega) = \mathrm{IM}_1(\mathbf{x}_R;\omega) + \mathrm{IM}_2(\mathbf{x}_R;\omega) + \cdots + \mathrm{IM}_n(\mathbf{x}_R;\omega) = \sum_{j=1}^{n} \mathrm{IM}_j(\mathbf{x}_R;\omega). \tag{12}$$

where p_0^j is the primary waves reflected from the j-th interface. $\mathrm{IM}_j(\mathbf{x}_R;\omega)$ denotes internal-multiples which are produced by the j-th multiple-generator and corresponding shallower generators. With this notation, for generator ($j = 0$), the shallowest generator, located at depth z_0, no generators shallower than it are existed, so no internal-multiples are generated from shallower layers; for generator ($j = 1$), located at depth z_1, internal-multiples are generated by generator-pair located at depth z_0 and z_1; while for generator ($j = 2$), located at depth z_2, internal multiples are generated by two generator-pairs: one located at depth z_0 and z_2, and the other at depth z_1 and z_2. With the same argument, for generator ($j = n$), the deepest generator, located at depth z_n, related internal multiples are generated by n generator-pairs, located at depth z_j ($j = 0, 1, 2, \ldots, n-1$) and z_n, respectively. As we can see, in this way, internal multiples, for any generator ($j > 0$), are generated from j generator-pairs, which consist of the j-th generator and all other shallower generators. In following, we prove that, when depth extrapolated to the j-th generator, internal-multiples generated by such j generator-pairs are all directly and adaptively eliminated beneath the j-th generator.

As the two-way wave equation based wavefield depth extrapolation performed, we have

$$\begin{cases} p(\mathbf{x}_j;\omega) = e^{-ik_z z_j}[p_u(\mathbf{x}_R;\omega) + \mathrm{IM}(\mathbf{x}_R;\omega)] + e^{+ik_z z_j}[p_u(\mathbf{x}_R;\omega) + \mathrm{IM}(\mathbf{x}_R;\omega)] \\ q(\mathbf{x}_j;\omega) = e^{-ik_z z_j}[p_u(\mathbf{x}_R;\omega) + \mathrm{IM}(\mathbf{x}_R;\omega)] - e^{+ik_z z_j}[p_u(\mathbf{x}_R;\omega) + \mathrm{IM}(\mathbf{x}_R;\omega)] \end{cases} \tag{13}$$

During each extrapolated depth, the primary and internal

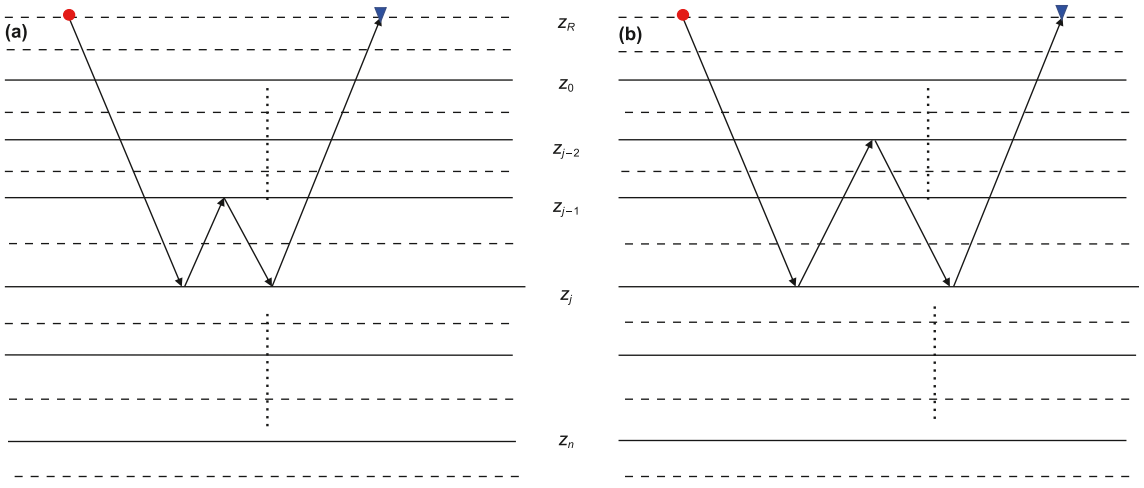

Fig. 2. Illustration of ray-path of internal multiples, and subsurface multiple-generators. Red circle denotes source, and blue triangle denotes receiver. Horizontal dash lines denote depth-steps of extrapolation; while horizontal solid lines represent multiple-generators. **(a)** Internal multiples are generated by generators at $z_{j-1}$and z_j; **(b)** internal multiples are generated by generators at z_{j-2} and z_j. Internal multiples generated by the j-th generator and corresponding shallower generators are, recorded at the measurement surface at z_R, denoted by IM_j in text. The vertical dash lines present numerous interfaces which can be used to generate internal multiples.

multiples separate into its up-going and down-going component, respectively. Thus, we have

$$\begin{cases} p(\mathbf{x}_j;\omega) = p_{\mathrm{u}}^{\mathrm{u}}(\mathbf{x}_j;\omega) + p_{\mathrm{u}}^{\mathrm{d}}(\mathbf{x}_j;\omega) + \mathrm{IM}^{\mathrm{u}}(\mathbf{x}_j;\omega) + \mathrm{IM}^{\mathrm{d}}(\mathbf{x}_j;\omega) \\ q(\mathbf{x}_j;\omega) = p_{\mathrm{u}}^{\mathrm{u}}(\mathbf{x}_j;\omega) - p_{\mathrm{u}}^{\mathrm{d}}(\mathbf{x}_j;\omega) + \mathrm{IM}^{\mathrm{u}}(\mathbf{x}_j;\omega) - \mathrm{IM}^{\mathrm{d}}(\mathbf{x}_j;\omega) \end{cases} \tag{14}$$

where $p_{\mathrm{u}}^{\mathrm{u}}(\mathbf{x}_j;\omega) = \mathrm{e}^{-ik_z z_j} p_{\mathrm{u}}(\mathbf{x}_{\mathrm{R}};\omega)$, $p_{\mathrm{u}}^{\mathrm{d}}(\mathbf{x}_j;\omega) = \mathrm{e}^{+ik_z z_j} p_{\mathrm{u}}(\mathbf{x}_{\mathrm{R}};\omega)$,

$\mathrm{IM}^{\mathrm{u}}(\mathbf{x}_j;\omega) = \mathrm{e}^{-ik_z z_j}\mathrm{IM}(\mathbf{x}_{\mathrm{R}};\omega)$, $\mathrm{IM}^{\mathrm{d}}(\mathbf{x}_j;\omega) = \mathrm{e}^{+ik_z z_j}\mathrm{IM}(\mathbf{x}_{\mathrm{R}};\omega)$.

It can be proved that internal multiples (generated by generator at $\mathbf{x}_j$ and corresponding shallower generator at $\mathbf{x}_0$), $\mathrm{IM}^{\mathrm{u}}(\mathbf{x}_j;\omega)$, are cancelled, beneath generator $\mathbf{x}_j$, by up-going wave component of transmitted down-going wavefield, $p_{\mathrm{u}}^{\mathrm{d}}(\mathbf{x}_j;\omega)$ (referring to Appendix A for details).

Therefore, we obtain

$$\begin{cases} p(\mathbf{x}_j;\omega) = p_{\mathrm{u}}^{\mathrm{u}}(\mathbf{x}_j;\omega) + \mathrm{IM}^{\mathrm{d}}(\mathbf{x}_j;\omega) \\ q(\mathbf{x}_j;\omega) = p_{\mathrm{u}}^{\mathrm{u}}(\mathbf{x}_j;\omega) - \mathrm{IM}^{\mathrm{d}}(\mathbf{x}_j;\omega) \end{cases} \tag{15}$$

Applying the up/down wavefield separation via the addition operation of Eq. (15), it can be rewritten as follows:

$$p'(\mathbf{x}_j;\omega) = p_{\mathrm{u}}^{\mathrm{u}}(\mathbf{x}_j;\omega) \tag{16}$$

2.2.3. Main feature of internal-multiple-elimination method

It is noted that, different from most of other internal multiple elimination schemes, our proposed method completes internal multiple elimination, not at the measurement surface but at some depth steps of two-way wave equation depth-extrapolation. Because of this, the challenging internal-multiple-elimination task, in our method, is separated to and adaptively completed at several different depth steps where internal multiple generators exist; and at those depth steps, only internal multiples, which are generated by the generator at current extrapolation depth and corresponding shallower generators, are eliminated. With this "task-distributed" implementation mechanism, internal-multiple-elimination processing in our proposed method becomes much simpler, comparing with most of sophisticated iterative-prediction based internal-multiple-elimination algorithms.

As described above, the primary feature of our proposed approach is efficiently, and just performing conventional two-way wave equation depth-extrapolation (according to Eqs. (1) and (2)), with suitable boundary conditions (as defined in Eq. (6)) and associated up/down wavefield separation (using Eqs. (4) and (7)), we can obtain needed up-going wavefields (primary waves) at each depth-extrapolation step (using Eq. (16)). For depth steps, where no multiple-generator is existed, the up-going wavefield obtained is same as that obtained from conventional two-way depth-extrapolation, without multiple-elimination processing; while for depth steps, where multiple-generators are existed, the up-going wavefield obtained is free of multiple interferences, with internal-multiples adaptively eliminated beneath corresponding multiple generators (as described by Eq. (15)). Because of this feature, the proposed method is very efficient for IME, without need of source wavelet and iterative prediction; and highly cost-effective for IMEM, being able to complete IME and IMEM two processing in same two-way depth-extrapolation scheme (as described in next subsection).

2.3. Internal-multiple-eliminated-migration

It is well known that internal multiples recorded at shallow depths normally produce imaging artifacts at deeper depths. Since all internal-multiples generated by multiple-generators, consisting of the current generator and corresponding shallower generators, have been eliminated during two-way depth-extrapolation. In performing the source wavefield depth extrapolation using Eq. (1) or Eq. (3) with Eq. (7) as the boundary condition, we generally have $p_s(\mathbf{x};\omega)$ and $q_s(\mathbf{x};\omega)$. By using efficient wavefield separation (with Eq. (8)), we only need to keep the down-going part of the source wavefield at each extrapolated depth. Since only the down-going component remains, we avoid the mutual coupling effect between up- and down-going waves in the source wavefields. Consequently, IME cannot generate internal multiples in the source wavefield. When performing the two-way wave equation-based depth extrapolation for source and receiver wavefields, the source wavefields include both up-going and down-going components, while the receiver wavefields contain the corresponding up-going

and down-going components. Using the conventional cross-correlation imaging condition typically generates low-frequency noise. However, by employing efficient wavefield separation (as described in Eq. (8)), the final imaging results are derived from the cross-correlation of the source down-going wavefields and the receiver up-going wavefields, effectively eliminating the low-frequency noise. Therefore, our proposed method can realize IMEM just by applying a conventional imaging condition at each depth. We can cross-correlate depth-extrapolated up-going wavefield (via backward extrapolation of the receiver wavefield) with down-going wavefield (via forward extrapolation of the source wavefield) as follows:

$$I_{\mathrm{IME}}(\mathbf{x}) = \sum_{\omega} s_{\mathrm{d}}(\mathbf{x};\omega) p'_{\mathrm{u}}(\mathbf{x};\omega) \tag{17}$$

where $I_{\mathrm{IME}}(\mathbf{x})$ denotes the imaging result with internal-multiples eliminated; $s_{\mathrm{d}}(\mathbf{x};\omega)$ represents down-going wavefield of source, and $p'_{\mathrm{u}}(\mathbf{x};\omega)$ represents up-going wavefield of receiver, free of internal-multiples. Using Eq. (17), IMEM is achieved.

2.4. Algorithm of proposed internal-multiple-elimination (IME) and internal-multiple-eliminated-migration (IMEM)

Based on above derivation and description, the algorithm of proposed IME and IMEM involves following key elements and steps:

1. Input data is similar to that of conventional migration: source signature (needed for migration only but not for IME), macro velocity model, and receiver data (with SRME processed);
2. Depth-extrapolating receiver data, with two-way wave equation depth-extrapolation scheme (Eqs. (1) and (2)) and up-going-wavefield-only boundary conditions using Eq. (6);
3. Adaptively completing internal-multiples-elimination at each depth-extrapolation step, based on Eqs. (4), (8) and (16);
4. Performing internal-multiple-eliminated-migration at each depth-extrapolation step, using conventional cross-correlation imaging condition, with Eq. (17);
5. Depth-extrapolating from depth $z = 0$ to the maximum depth $z_{\max} = n \times dz$, yielding imaging results free of internal-multiple artifacts, for all depth steps.

As we can see that the algorithm of our proposed method and its computational cost, for completing internal-multiple-elimination and such related migration, is same as that of conventional two-way wave equation depth-extrapolation based migration. Although the proposed method is proved to be accurate for horizontally homogeneous layered media, numerical examples in next segment illustrate that the method is also suitable and valid for horizontally layered media with moderately lateral variations.

3. Numerical examples

In this segment, we use several synthesized data models and a real field data to assess the validity and effectiveness of our proposed approach for internal-multiple-elimination, and internal-multiple-eliminated-migration. To create shot gathers containing internal multiples, we employ the finite difference technique to solve acoustic wave equation. In seismic modeling, we incorporate absorbing layers in velocity models, to be consistent with the assumption that surface-related multiples have been effectively attenuated from input data.

3.1. One dimensional model for illustration

Efficient up/down decomposition of wavefields is intensively used, at each depth-extrapolation step, in the proposed method. To demonstrate simplicity and efficiency of this operation in our method, we create and use a horizontally layered model for illustration. The model features a background velocity of 1500 m/s, and includes two interfaces (with velocity 3000 m/s) positioned at depths of $z = 250$ m and 750 m, respectively. We use a Ricker wavelet, with a dominant frequency of 20 Hz, as a boundary condition for pressure, and the pressure derivative wavefield, $\partial p/\partial z$, being zero for another boundary condition.

The depth-extrapolated pressure wavefields ($p(\mathbf{x};\omega)$, $p_z(\mathbf{x};\omega)$ and $q(\mathbf{x};\omega)$), using two-way depth-extrapolation scheme (Eqs. (1), (2) and (6)), are calculated and depicted in Fig. 3(a)–(c), respectively. These two-way wavefields are separated to their one-way counterparts: up-going and down-going wavefields ($p_{\mathrm{u}}(\mathbf{x};\omega)$ and $p_{\mathrm{d}}(\mathbf{x};\omega)$) at each depth-extrapolation step, via a simple summation operation (Eq. (8)), as shown in Fig. 3(d), (e). With the same method, wavefield decomposition of $p_{\mathrm{u}}(\mathbf{x};\omega)$ can be performed, leading to its separated up-going and down-going components: $p^{\mathrm{u}}_{\mathrm{u}}(\mathbf{x};\omega)$ and $p^{\mathrm{d}}_{\mathrm{u}}(\mathbf{x};\omega)$, as shown in Fig. 3(f), (g), respectively. From Fig. 3, it is seen that one-way propagators can be accurately and efficiently calculated through two-way wave equation based depth-extrapolation scheme and associated efficient up/down wavefield separation (You and Cao, 2020; You et al., 2022), which is a key feature and superiority of our proposed approach.

To assess the validity and efficiency of the proposed method in successfully eliminating internal multiples, we carry out a seismic wavefield simulation utilizing one-dimensional acoustic wave equation. An absorbing layer is situated atop the model to mitigate influences of surface-related-multiple waves. Fig. 4(a) displays recorded seismic signals, with direct wave muted. In our velocity model, the background velocity is 1500 m/s, while three interfaces (with velocity of 3000 m/s) are located at $z = 250$ m, 400 m, and 750 m, respectively. Reflection waves are recorded at $z = 0$; and simulated wavefield propagation (in time-space domain), using a Ricker wavelet with dominant frequency of 20 Hz, are shown in Fig. 4(b). In Fig. 4(b), we can distinguish three primary waves (denoted by P1, P2, and P3) reflected from three interfaces respectively, and four internal multiples (denoted by IM1, IM2, IM3, and IM4), generated by wavefield interactions of three interfaces. It can be seen also that IM1 is generated by the first two interfaces (generators), while IM2, IM3, and IM4 are generated by generators consisting of the third interface and other two shallower interfaces.

To illustrate internal-multiple-elimination mechanism of proposed method, we calculate five different depth-extrapolated wavefields by using five different input data: P2+IM1, P2+IM1+P3, P2+IM1+P3+IM2, P2+IM1+P3+IM2+IM3 and P2+IM1+P3+IM2+IM3+IM4. The five depth-extrapolated wavefields are displayed in Fig. 5(a)–(e), respectively. According to test results in Fig. 5(a)–(e), we can observe that internal multiple IM1 is eliminated beneath the second interface by using input data P2+IM1 or P2+IM1+P3, as shown in Fig. 5(a), (b), while internal multiples involving IM2, IM3 and IM4 are eliminated beneath the third interface by using input data P2+IM1+P3+IM2, P2+IM1+P3+IM2+IM3 and P2+IM1+P3+IM2+IM3+IM4, respectively, as shown in Fig. 5(c)–(e). Internal multiple elimination areas are marked by the dashed black circles in Fig. 5(a)–(e). The test results of Fig. 5(a)–(e), verify one of main features of the proposed method: that is, when data is depth-extrapolated to any depth where related interface is a multiple generator, internal multiples—generated by the generator and corresponding shallower generators—are adaptively eliminated beneath the generator (and

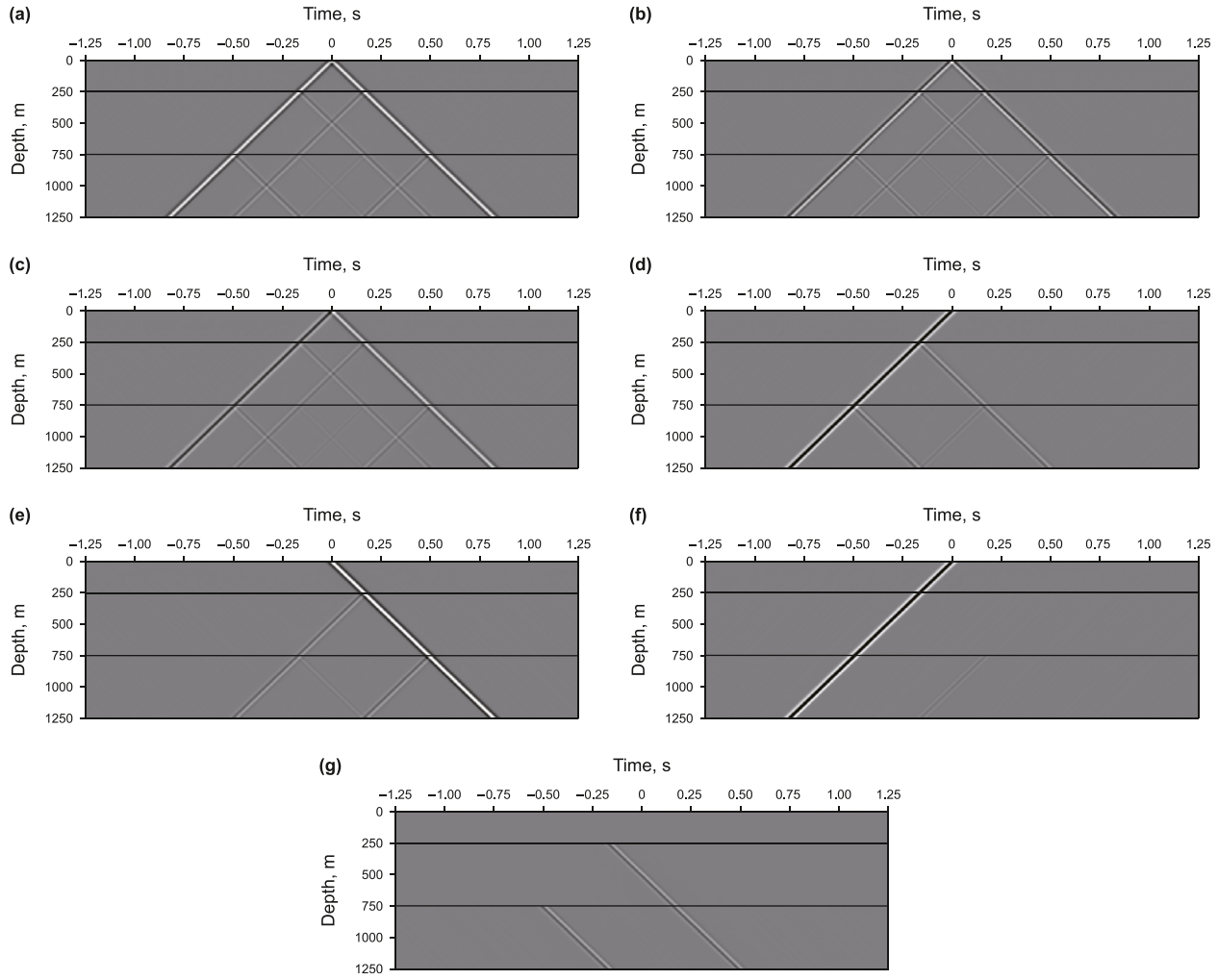

Fig. 3. Depth-extrapolated wavefields at **x**: **(a)** pressure wavefield $p(\mathbf{x};\omega)$; **(b)** pressure derivative wavefield $p_z(\mathbf{x};\omega)$; **(c)** pressure wavefield $q(\mathbf{x};\omega)$; **(d)** up-going wavefield $p_u(\mathbf{x};\omega)$; **(e)** down-going wavefield $p_d(\mathbf{x};\omega)$; **(f)** up-going component $p_u^u(\mathbf{x};\omega)$; **(g)** down-going component $p_u^d(\mathbf{x};\omega)$. Wavefields presented in Fig. 3(a), (b) are obtained using Eq. (1), while wavefields in Fig. 3(c) are obtained using Eq. (4). It is noted that the up-going wavefields in Fig. 3(a), (c) have opposite phases, whereas the down-going wavefields share the same phases. Wavefields presented in Fig. 3(d), (e) are obtained using efficient wavefield separation (with Eq. (8)), but each still contains both up- and down-going components. Wavefields presented in Fig. 3(f), (g) are further refined using efficient wavefield separation (with Eq. (8)), producing separate up- and down-going components.

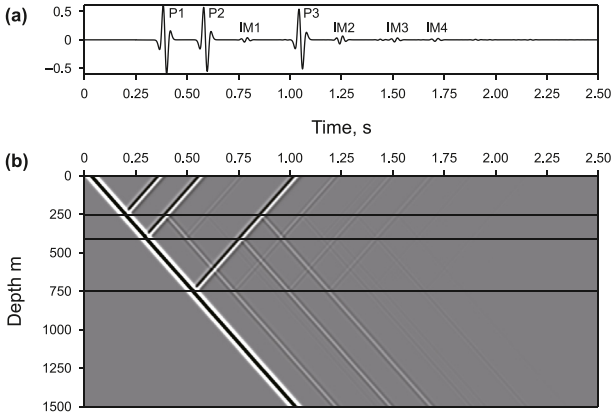

Fig. 4. **(a)** Recorded reflection waves at the surface, and **(b)** the diagram of wavefield propagation in time-space domain. Black lines in (b) represent the interfaces. Note that the direct wave is muted in Fig. 4(a). P1, P2 and P3 denote the primary reflected waves from the three interfaces, respectively. IM1 is generated by the first two interfaces (generators); IM2, IM3, and IM4, on the other hand, are generated by the third interface in combination with the two shallower interfaces, respectively.

related depth). In this example, IM1 is eliminated beneath the second interface (depth of 400 m), while IM2, IM3, and IM4 are all adaptively eliminated beneath the third interface (depth of 700 m). It is worth noting, however, that above tests are for illustration purpose only; in processing practice, all recorded reflections (P2+P3+IM1+IM2+IM3+IM4) are used as input data, therefore, actual depth-extrapolated wavefield utilizing our proposed approach is same as that of Fig. 5(e). As a comparison, the depth-extrapolated up-going wavefield using conventional depth extrapolation strategy (You and Cao, 2020; You et al., 2022), is shown in Fig. 5(f), which does not eliminate the internal multiples.

To verify the effectiveness of our proposed method in eliminating the influence of internal multiples on imaging, we compare imaging results, with and without internal multiple impacts, as depicted in Fig. 6. Evidently, crosstalk artifacts are observed in imaging using conventional depth-extrapolation scheme without internal multiple elimination, as indicated by black arrows in Fig. 6(a). Conversely, imaging using our proposed method exhibits good performance in removing the impact of all four sets of internal multiples, as displayed in Fig. 6(b). This demonstrates effectiveness of our proposed method in adaptive elimination of internal multiples.

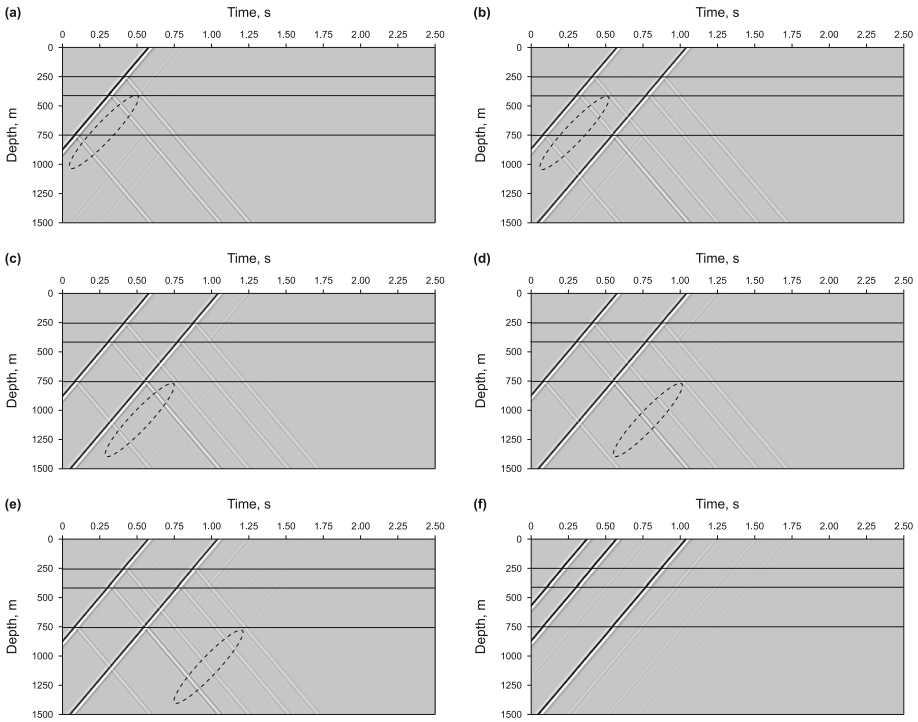

Fig. 5. Depth-extrapolated wavefields by using the proposed depth extrapolation scheme, with different input data: **(a)** P2+IM1, **(b)** P2+IM1+P3, **(c)** P2+IM1+P3+IM2, **(d)** P2+IM1+P3+IM2+IM3, **(e)** P2+IM1+P3+IM2+IM3+IM4; and **(f)** depth-extrapolated up-going wavefield by using the conventional depth extrapolation scheme.

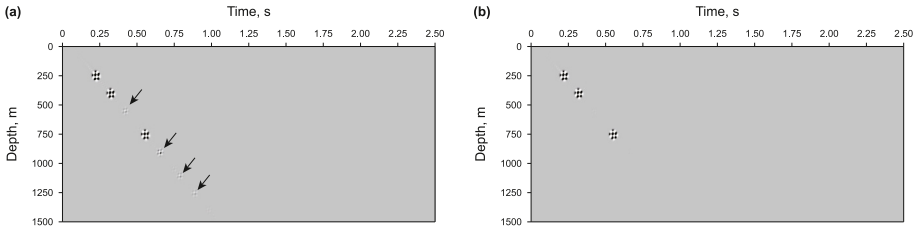

Fig. 6. Imaging results: **(a)** without internal-multiple-elimination using conventional depth-extrapolation scheme (imaging artifacts pointed by black arrows are produced by internal multiples); **(b)** with internal-multiple-elimination using our proposed method.

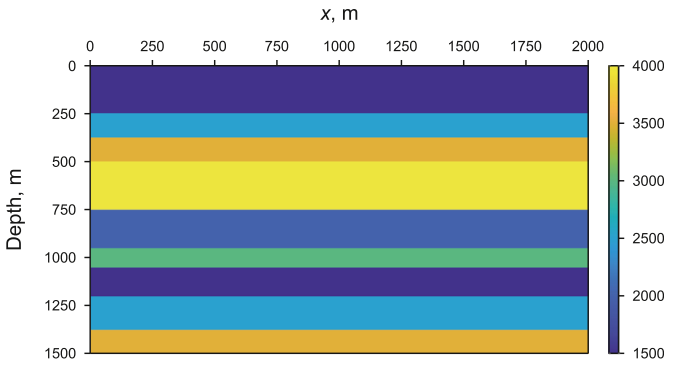

Fig. 7. Horizontal layered velocity model.

3.2. Horizontal layered model

In order to further verify performance of the proposed method, we establish a nine-layer horizontal layered model, as displayed in Fig. 7. Dimensions of the model are 1500 m × 2000 m, with grid spacings of 2.5 m in both horizontal and vertical directions. Seismic data acquisition employs a fixed spread, with receivers and a source both positioned at depth = 0. The simulation includes a grand total of 100 shot gathers, with 200 receivers in each gather; the intervals between sources and receivers are 20 m and 10 m, respectively. A Ricker wavelet serves as the source function, featuring a dominant frequency of 30 Hz and a time-sampling interval of 0.0005 s. To identify the internal multiples, the conventional one-way phase-shift-plus-interpretation (PSPI) propagator is employed to generate the reflection waves without internal multiples. For a fair comparison, the shot gathers generated using the one-way PSPI propagator and the conventional finite difference method are shown in Fig. 8. In the shot gather produced by the conventional finite difference method, the internal multiples are indicated by black arrows, as shown in Fig. 8(b).

For imaging comparison, we perform depth extrapolation and migration using two-dimensional shot gather data. To assess the performance of the proposed method in internal-multiple-elimination and internal-multiple-eliminated-migration, we compare it with conventional phase-shift depth migration. The outcomes of the migration are displayed in Fig. 9. As we can see that obvious imaging artifacts are existed in conventional depth migration result, as displayed in Fig. 9(a), and indicated by black

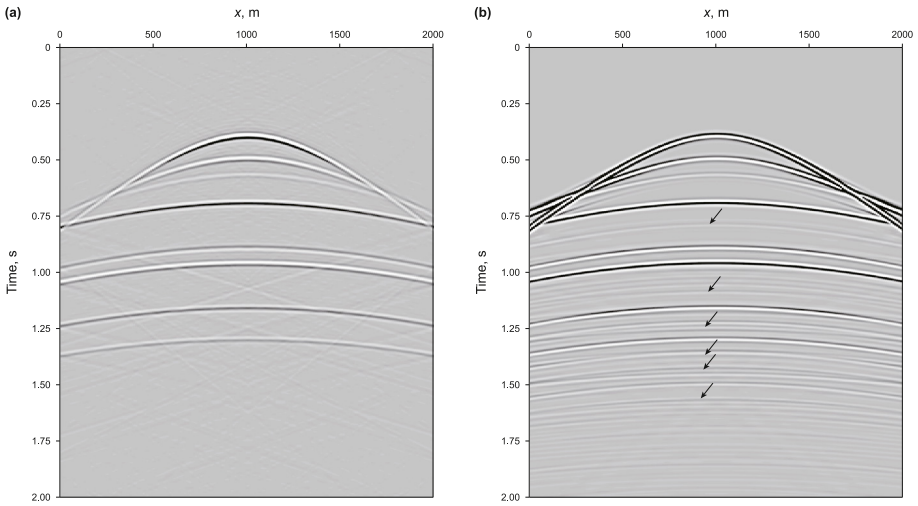

Fig. 8. Shot gather produced by using **(a)** one-way phase-shift-plus-interpretation (PSPI) propagator and **(b)** conventional finite-difference method. shot gather containing internal multiples which are pointed by black arrows.

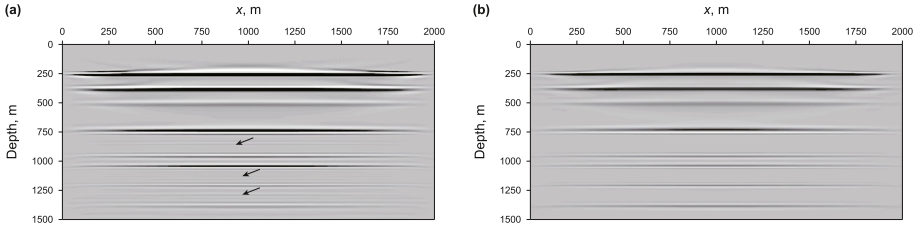

Fig. 9. Imaging results by using different methods: **(a)** conventional depth migration method without internal multiples elimination; **(b)** our proposed method with adaptive internal multiples elimination. The black arrows indicate the imaging artifact produced by internal multiples.

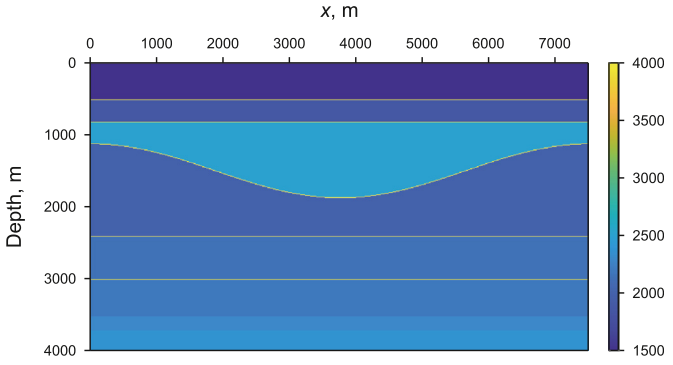

Fig. 10. Velocity function of multi-layer model.

arrows; the artifacts are caused by severe internal multiples, generated from many "two-interface" generators in this model. In contrast, our proposed method successfully eliminates internal multiples and achieves much clearer imaging, as shown in Fig. 9(b).

3.3. Multi-layer model with a curved layer

Fig. 10 shows a complex structural model that is frequently used in internal-multiple-elimination related tests (e.g., Lomas and Curtis, 2019; Ravasi and Vasconcelos, 2021). The size of model is 4000 m × 7500 m, with grid spacing of 10.0 m in both horizontal and vertical directions. In total, there are 188 shot gathers, and each shot gather has 375 receivers. Sources and receivers are uniformly spread across the model's top surface, with intervals of 40.0 m and 20.0 m, respectively. The source function employs a Ricker wavelet with a dominant frequency of 20 Hz. The maximum recording period spans around 6.0 s, with a sampling interval of 0.001 s. To indicate the internal multiples produced by interfaces, the shot gather using the one-way PSPI propagator is generated, for comparison with the shot gather of the conventional finite difference method, as shown in Fig. 11.

A test is conducted on this model to further evaluate the availability of our suggested method in eliminating internal multiples. For this evaluation, we compare conventional PSPI method (Gazdag and Sguazzero, 1984), which does not include internal multiple elimination, with our proposed method, by migrating all shot gathers. The migration results using these two methods are presented in Fig. 12(a), (b), respectively. Owing to the existence of internal multiples, the conventional PSPI method exhibits artifacts in imaging, as denoted by black arrows in Fig. 12(a). Obviously, these imaging artifacts can potentially lead to incorrect seismic interpretation. In contrast, our proposed method accurately eliminates internal multiples, resulting in a significantly improved imaging, as displayed in Fig. 12(b).

3.4. SEG/EAGE salt model

In this numerical example, we test and evaluate our method on a complex SEG/EAGE salt model, which is displayed in Fig. 13. The salt model has dimensions of 2200 m × 6000 m, with a grid spacing of 10.0 m in both horizontal and vertical directions. In our seismic acquisition scheme, we position 600 receivers along the surface at intervals of 10.0 m, and 150 sources along the surface at intervals of 40.0 m. The maximum recording time extends to about 4.0 s, with a

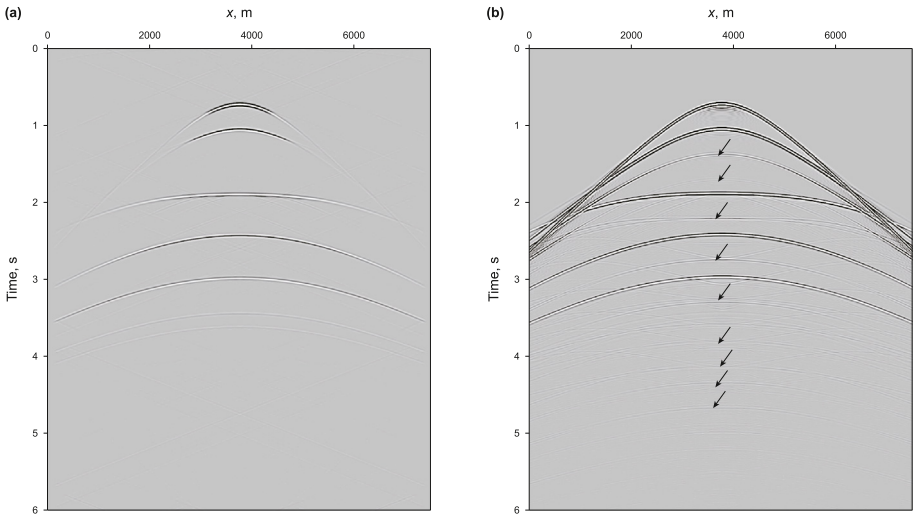

Fig. 11. Shot gather produced by using **(a)** one-way PSPI propagator and **(b)** conventional finite-difference method. shot gather containing internal multiples which are pointed by black arrows.

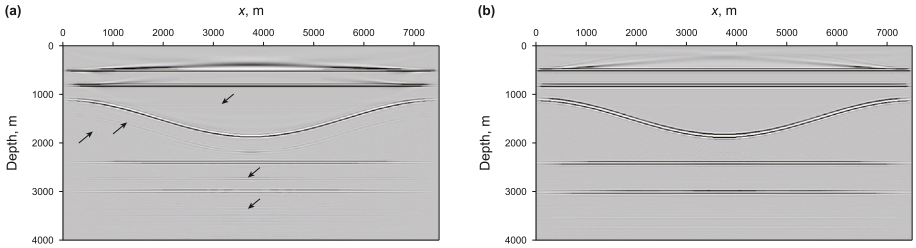

Fig. 12. Imaging results by using different methods: **(a)** conventional PSPI method without internal multiples elimination; **(b)** our proposed method with adaptive internal multiples elimination. The black arrows indicate imaging artifacts produced by internal multiples.

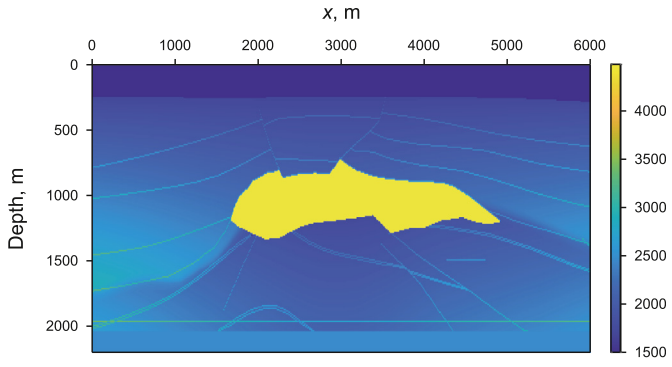

Fig. 13. Salt velocity model.

sampling interval of 0.001 s.

Because of presence of a salt body, and a significant velocity difference (in the middle part of section), internal multiples associated with the salt dome are generated, and present a significant challenge to imaging quality. To address this challenge, and evaluate our proposed method, we employ and test both conventional RTM and our proposed IMEM methods for imaging the salt model. Fig. 14(a), (b) respectively depict the imaging results obtained from the two methods. Fig. 14(a) reveals imaging artifacts beneath the salt dome, as indicated by black arrows, which diminish the imaging quality of conventional RTM method. In contrast, Fig. 14(b) presents a much clearer imaging result beneath the salt dome by effectively eliminating internal multiples during depth extrapolation. This numerical result verifies the accuracy and efficiency of

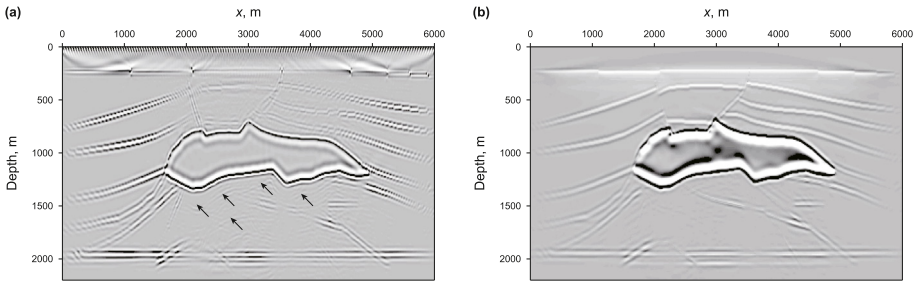

Fig. 14. Imaging results obtained by using different methods: **(a)** conventional RTM method and **(b)** our proposed method.

the proposed approach in attenuating internal multiples, and achieving high-quality imaging (free of internal multiple interferences), even within subsurface media exhibiting pronounced lateral velocity variations. It is worthwhile to emphasize that the proposed approach is highly efficient because internal-multiple-elimination and internal-multiple-eliminated-migration are naturally integrated into the same two-way wave equation depth-extrapolation scheme, without special requirements for positions of sources and receivers being co-located, and additional computational cost (comparing with conventional two-way depth-extrapolation based migration).

3.5. Real data application

To evaluate the performance of our proposed method with real data, we collected real shot gathers from a carbonate reservoir zone. Within these geological strata, certain formations bearing carbonate have relatively high velocity values, which are integrated into the geological structure. These carbonate-bearing formations enhance the generation of internal multiples during seismic wave propagation. The inverted velocity model and a shot gather are depicted in Fig. 15, where the shot gather suffers from severe background noise, substantially degrading the signal-to-noise ratio of the seismic data. This combination of internal multiples and background noise presents a significant challenge in achieving a clear imaging section. However, by employing both conventional one-way PSPI migration and our method to process the shot gathers, we observed distinct imaging results, as illustrated in Fig. 16. For a clear comparison, the partial enlarged sections of their results are shown in Fig. 17. The imaging result of the conventional one-way PSPI migration method is heavily affected by internal multiples, with imaging crosstalk from these multiples obscuring true imaging events and complicating the identification and interpretation of such events. Conversely, our method, through the application of IME, allows for the clear observation and identification of some imaging events in its imaging section, highlighted by the dashed black circle in Fig. 17, demonstrating a marked improvement in imaging quality over the conventional method. This case underlines the capability of our method to suppress internal multiples and enhance imaging quality effectively.

4. Discussion

4.1. Velocity sensitivity analysis

As depicted in the theory section, the elimination of internal multiples using a two-way wave equation wavefield depth extrapolation scheme depends on the reflection coefficients of structures, enabling adaptive internal multiple elimination (IME). This necessitates evaluating the IME performance of our proposed method with smoothed velocity models, such as those using inaccurate velocity data. In our cases, the 3×3 and 7×7 Gaussian windows are applied to the SEG/EAGE Salt model for smoothing the original velocity model, as illustrated in Fig. 18. A larger filtering window blurs the structures more, making finer interfaces and the boundary of the salt dome become less discernible, as shown in Fig. 18. We use conventional RTM and our proposed methods to evaluate imaging performance with these smoothed velocity models, as shown in Figs. 19 and 20. The use of inaccurately modeled velocities affects IME performance, generating some imaging crosstalks beneath the Salt dome, as pointed out the results seen in Fig. 14. However, our proposed IME method outperforms conventional RTM methods by partially eliminating internal multiples and reducing imaging artifacts of internal multiples, as indicated by the dashed yellow circles in Figs. 19 and 20. For a quantitative assessment, we extracted imaging amplitudes at $x = 3000$ m from migration sections derived from the original and the smoothed velocity models (3×3 and 7×7 Gaussian windows), as plotted in Fig. 21. The comparison of imaging amplitudes of internal multiples beneath the salt dome, magnified in Fig. 21, reveals that enhancing the smoothness of the velocity model results in a gradual rise in the false imaging amplitude of internal multiples. Yet, our method substantially diminishes the effect of internal multiples. Our method demonstrates significant success in suppressing internal multiples within accurate velocity structures and achieves partial suppression with smoothed velocity models. Eliminating internal multiples in complex media structures remains a challenge, further research will focus on suppressing internal multiples between structures in either smoothed velocity models or complex conditions, paving a new path for internal multiple elimination by using two-way wave equation based wavefield depth extrapolation.

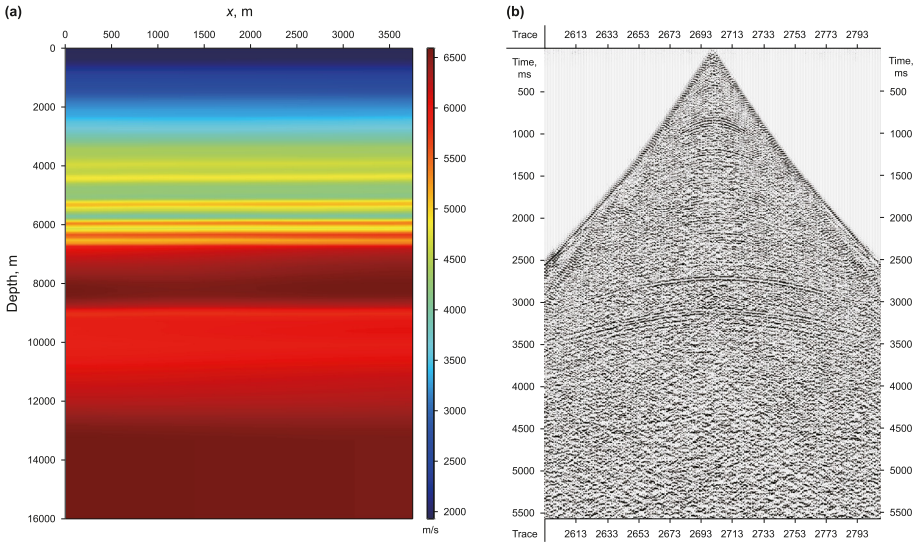

Fig. 15. **(a)** Velocity model; **(b)** shot gather.

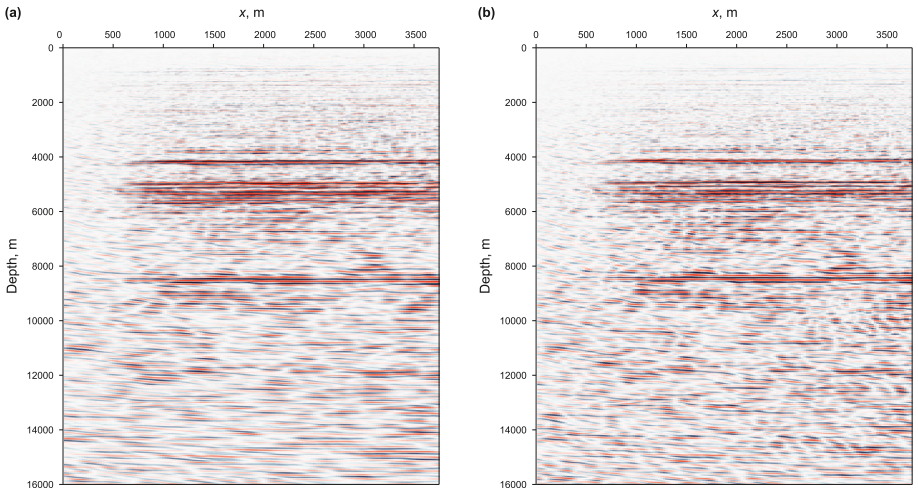

Fig. 16. Imaging result by using **(a)** the conventional one-way PSPI migration method; **(b)** our proposed method.

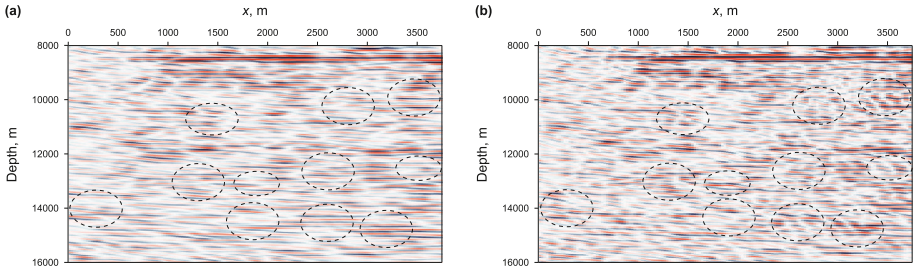

Fig. 17. Partial enlarged imaging result by using **(a)** the conventional one-way PSPI migration method; **(b)** our proposed method.

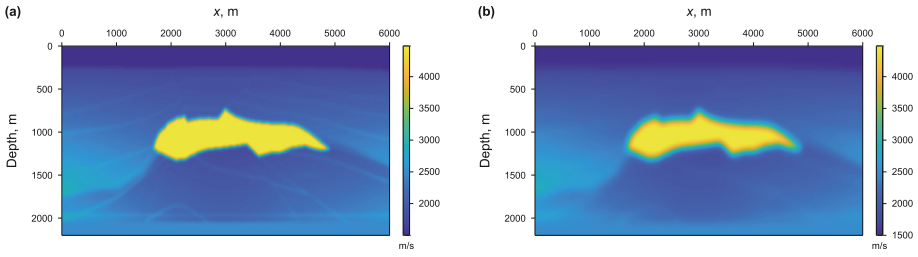

Fig. 18. Smoothed original velocity model by using gaussian filter with **(a)** 3 × 3 window; **(b)** 7 × 7 window.

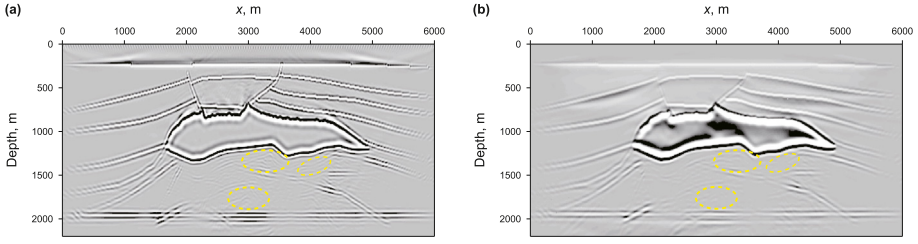

Fig. 19. Imaging results obtained using the smoothed velocity with 3 × 3 Gaussian windows: **(a)** RTM; **(b)** our proposed method.

4.2. Computational time analysis

To compare the computational efficiency of the proposed method in handling internal multiples and wavefield extrapolation, we provide statistics on the computation time for the two-way wave equation-based depth extrapolation scheme with and without IME in the numerical model to migrate one shot gather, as listed in Table 1. From the computation time of the numerical examples, it is evident that the internal multiple elimination does not add extra computational load to the two-way wave equation-based

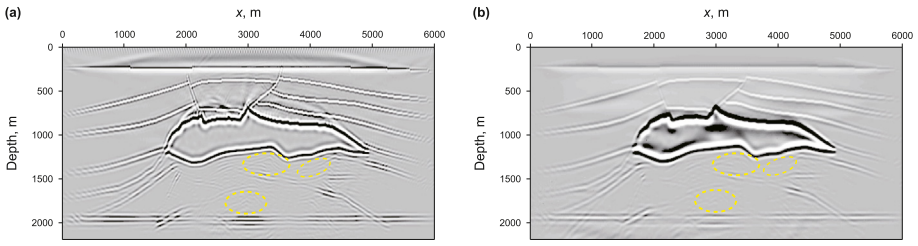

Fig. 20. Imaging results obtained using the smoothed velocity with 7 × 7 Gaussian windows: **(a)** RTM; **(b)** our proposed method.

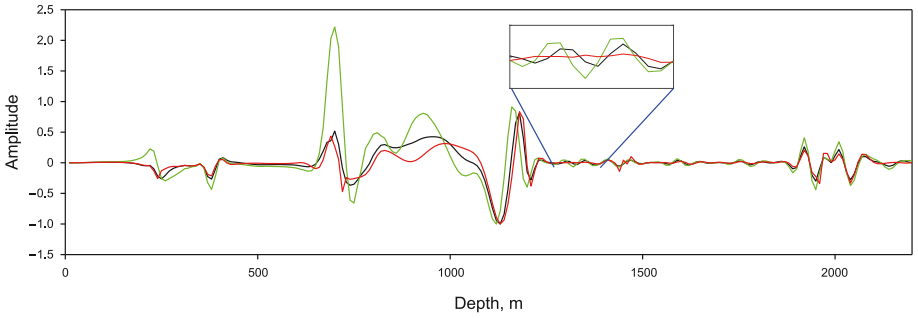

Fig. 21. Imaging amplitude extracted at $x = 3000$ m from migration sections of our proposed method using different velocity models: red line presents the original velocity model, while black and green lines denote the smoothed velocity with 3 × 3 and 7× 7 gaussian filtering windows, respectively.

Table 1
Comparison of computational times (unit: s) between two-way wave-equation-based depth extrapolation (TWDE) scheme with and without IME.

Model	Horizontal layered model	Multi-layer model with a curved layer	SEG/EAGE Salt model
Computational times of TWDE with IME, s	61	45	304
Computational times of TWE without IME, s	59	40	214

depth extrapolation. This is because the method developed in this paper naturally integrates the internal multiple elimination into the two-way wave equation-based depth extrapolation scheme.

5. Conclusions

To address the internal-multiple-elimination and internal-multiple-eliminated-migration challenges, in this study, we develop an adaptive internal-multiple-elimination scheme using two-way wave equation based wavefield depth-extrapolation. With two-way wave equation depth-extrapolation framework, suitable boundary conditions, and associated up/down wavefield separation mechanism, our proposed method enables up-going wavefields (input data) propagated, both backward and forward (in time) simultaneously, and internal-multiple-elimination completed adaptively and efficiently, at each depth-extrapolation step without need of source wavelet and iterative prediction computations. The input data for the proposed method is exactly same as that for conventional migration, without special requirements for source/receiver sampling and location. Moreover, our proposed method seamlessly integrates internal-multiple-elimination into two-way depth-extrapolation scheme and related migration, making the proposed internal-multiple-eliminated-migration highly efficient without requiring additional computational cost, compared with conventional two-way depth-extrapolation based migration. Numerical examples and the real data application, including tests on one-dimensional model, horizontal layered model, multi-layer model with a curved layer, and SEG/EAGE Salt model, verify and demonstrate that our proposed scheme can adaptively eliminate internal multiples during two-way depth extrapolation, effectively and efficiently, and meanwhile achieve high-quality imaging results without (or with much less) internal-multiple artifacts.

CRediT authorship contribution statement

Jia-Chun You: Writing – original draft, Investigation, Conceptualization. **Gu-Lan Zhang:** Software, Data curation. **Xing-Guo Huang:** Writing – review & editing, Validation. **Xiang-Wen Li:** Resources, Investigation. **Jun-Xing Cao:** Writing – review & editing, Formal analysis.

Declaration of competing interest

The authors declare that they have no known competing financial interests or personal relationships that could have appeared to influence the work reported in this paper.

Acknowledgements

We thank Dr. Nai-De Pan, editors and reviewers for their valuable and constructive suggestions, which greatly improved the manuscript. This research is financially supported by the National Natural Science Foundation of China (Grant No. 42004103), Sichuan Science and Technology Program (2023NSFSC0257), and the CNPC Innovation Found (2022DQ02-0306).

Appendix A

Proof and physical insight of Eq. (15)

To prove that our proposed method is able to eliminate internal multiples beneath multiple generators, as described by Eq. (15), we use one-dimensional "two interfaces" model for illustration. This model is schematically shown in Fig. A-1(a). For simplicity but without loss of generality, a pulse function, which is denoted as $\delta(t)$, is employed as a source, while two interfaces, positioned at depths z_0 and z_1, are used as an internal-multiple generator; the earth medium between the two interfaces is characterized by constant density and background velocity c. Since the thickness of two interfaces is $\Delta z = z_1 - z_0$, the corresponding one-way traveling time is $t = \Delta z/c$. For a down-going wave incident on interfaces from top, local reflection coefficients at depth level z_j $(j = 0, 1)$, are defined as r_j; while for an up-going wave incident on interfaces from below, they are defined as $-r_j$. For notation simplicity (without loss of accuracy), transmission coefficients at the interfaces are omitted. With these definitions in place, two primary waves P1 and P2, and one internal multiple wave IM are shown in Fig. A-1(a) (modified from Slob et al., 2014).

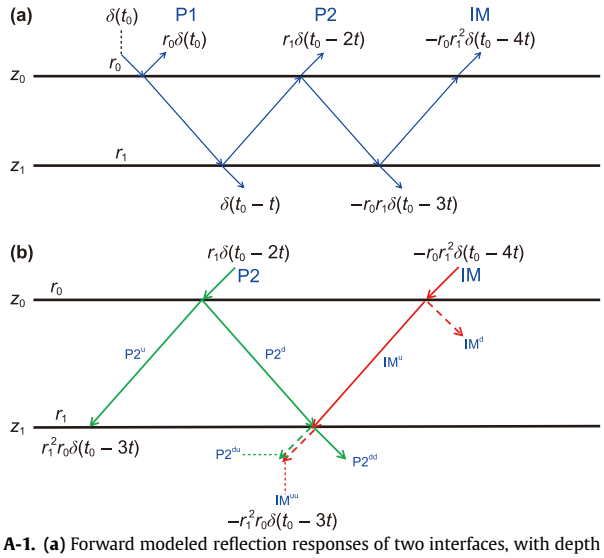

Fig. A-1. **(a)** Forward modeled reflection responses of two interfaces, with depth at z_0 and z_1 respectively; **(b)** reflection responses after depth-extrapolation from z_0 to z_1; rays (in green) are related to primary P2, while rays (in red) related to internal multiple IM; dashed lines for $\mathrm{P2}^{\mathrm{du}}(z_1;\omega)$ and $\mathrm{IM}^{\mathrm{uu}}(z_1;\omega)$ indicate that internal multiple is cancelled and eliminated beneath the second interface. Note that all transmission notations are omitted in this figure.

When primary wave (P2) and internal multiples (IM) are depth-extrapolated jointly from depth z_0 to z_1, using two-way depth-extrapolation scheme (with boundary conditions defined by Eq. (6)), resulted wavefields are shown in Fig. A-1(b). Notably, when primary wave P2 is depth-extrapolated from depth z_0 to z_1, based on Eq. (7), it generates not only backward propagated up-going wave $\mathrm{P2}^{\mathrm{u}}$ but also forward propagated down-going wave $\mathrm{P2}^{\mathrm{d}}$ as follows:

$$\mathrm{P2}^{\mathrm{u}}(z_1;\omega) = \mathrm{e}^{-ik_z\Delta z}\mathrm{P2}(z_0;\omega), \tag{A-1}$$

and

$$\mathrm{P2}^{\mathrm{d}}(z_1;\omega) = \mathrm{e}^{ik_z\Delta z}\mathrm{P2}(z_0;\omega). \tag{A-2}$$

With the same argument, when internal multiples IM is depth-extrapolated from depth z_0 to z_1, both up-going and down-going waves $\mathrm{IM}^{\mathrm{u}}(z_1;\omega)$ and $\mathrm{IM}^{\mathrm{d}}(z_1;\omega)$ are generated:

$$\mathrm{IM}^{\mathrm{u}}(z_1;\omega) = \mathrm{e}^{-ik_z\Delta z}\mathrm{IM}(z_0;\omega), \tag{A-3}$$

and

$$\mathrm{IM}^{\mathrm{d}}(z_1;\omega) = \mathrm{e}^{ik_z\Delta z}\mathrm{IM}(z_0;\omega). \tag{A-4}$$

As shown in Fig. A-1(b), arrival times at z_1, for wavefields $\mathrm{P2}^{\mathrm{d}}(z_1;\omega)$ and $\mathrm{IM}^{\mathrm{u}}(z_1;\omega)$, are same (referring to Eqs. (A-2) and (A-3)). It is noted also that, when down-going wave $\mathrm{P2}^{\mathrm{d}}(z_1;\omega)$ passes through interface at z_1, it generates two waves: a transmitted down-going wave $\mathrm{P2}^{\mathrm{dd}}(z_1;\omega)$, and an up-going wave $\mathrm{P2}^{\mathrm{du}}(z_1;\omega)$; and following relation between $\mathrm{P2}^{\mathrm{du}}(z_1;\omega)$ and $\mathrm{P2}^{\mathrm{d}}(z_1;\omega)$ is held:

$$\mathrm{P2}^{\mathrm{du}}(z_1;\omega) = -r_1\mathrm{P2}^{\mathrm{d}}(z_1;\omega), \tag{A-5}$$

where $-r_j$ is reflection coefficient of interface at z_1 (if incident wave hits interface from below), while transmission coefficient at z_1 is omitted. As seen from Fig. A-1, we also have following relation equations between $\mathrm{P2}^{\mathrm{d}}(z_1;\omega)$, $\mathrm{IM}^{\mathrm{u}}(z_1;\omega)$, and $\mathrm{IM}^{\mathrm{uu}}(z_1;\omega)$:

$$\begin{cases} \mathrm{IM}^{\mathrm{u}}(z_1;\omega) = r_1\mathrm{P2}^{\mathrm{d}}(z_1;\omega) \\ \mathrm{IM}^{\mathrm{uu}}(z_1;\omega) = \mathrm{IM}^{\mathrm{u}}(z_1;\omega) \end{cases}, \tag{A-6}$$

where $\mathrm{IM}^{\mathrm{uu}}(z_1;\omega)$ corresponds to transmitted $\mathrm{IM}^{\mathrm{u}}(z_1;\omega)$ (beneath interface at z_1), in second equation of Eq. (A-6); transmission coefficient is omitted. Using Eqs. (A-5) and (A-6), we can derive and obtain following equation:

$$\mathrm{P2}^{\mathrm{du}}(z_1;\omega) + \mathrm{IM}^{\mathrm{uu}}(z_1;\omega) = 0. \tag{A-7}$$

Since transmission coefficients are omitted for both $\mathrm{P2}^{\mathrm{du}}(z_1;\omega)$ and $\mathrm{IM}^{\mathrm{uu}}(z_1;\omega)$ in Eqs. (A-5), (A-6), and (A-7), it does not affect the derivation and accuracy of Eq. (A-7). From Eq. (A-7) and Fig. A-1(b), we can see that up-going waves, $\mathrm{P2}^{\mathrm{du}}(z_1;\omega)$ and $\mathrm{IM}^{\mathrm{uu}}(z_1;\omega)$, have same arrival times and magnitudes at z_1, but opposite polarities beneath depth z_1. Because of this, internal-multiples, $\mathrm{IM}^{\mathrm{uu}}(z_1;\omega)$, is cancelled and eliminated by up-going wave, $\mathrm{P2}^{\mathrm{du}}(z_1;\omega)$, generated beneath the multiple-generator interface, during two-way depth-extrapolation. With the above derivation and description of Eq. (A-7), we complete proof of Eq. (15).

It is worth noting that although above proof of Eq. (A-7), for simplicity reason, is only discussed for and based on two-interfaces located at depth of z_0 and z_1, it can be extended to any two-interface pairs located at depth $z_j = l_j dz - z_{\mathrm{R}}$ $(j = 0, 1, 2, \ldots, n)$, for horizontally homogeneous layered media, as developed and described in Theory section; and, with the same argument, Eq. (A-7) is established for higher orders of internal multiples too.

References

Araújo, F.V., Weglein, A.B., Carvalho, P.M., Stolt, R.H., 1994. Inverse scattering series for multiple attenuation: an example with surface and internal multiples. In: SEG Technical Program Expanded Abstracts 1994, pp. 1039–1041. https://doi.org/10.1190/1.1822691.

Behura, J., Wapenaar, K., Snieder, R., 2014. Autofocus imaging. Image reconstruction based on inverse scattering theory. Geophysics 79 (3), A19–A26. https://doi.org/10.1190/geo2013-0398.1.

Berkhout, A.J., Verschuur, D.J., 2005. Removal of internal multiples with the common-focus-point (CFP) approach: Part 1-Explanation of the theory. Geophysics 70 (3), V45–V60. https://doi.org/10.1190/1.1925753.

Broggini, F., Snieder, R., Wapenaar, K., 2012. Focusing the wavefield inside an unknown 1D medium: beyond seismic interferometry. Geophysics 77, A25–A28. https://doi.org/10.1190/geo2012-0060.1.

Broggini, F., Snieder, R., Wapenaar, K., 2014. Data-driven wavefield focusing and imaging with multidimensional deconvolution: numerical examples for reflection data with internal multiples. Geophysics 79 (3), WA107–WA115. https://doi.org/10.1190/geo2013-0307.1.

Chen, M., Liu, J.H., Cui, Y.F., Hu, T.Y., Chen, F.X., Kuang, W.K., Zhang, Z., 2018.

Poststack internal multiples attenuation based on virtual events. Appl. Geophys. 15 (3–4), 491–499. https://doi.org/10.1007/s11770-018-0694-5.
Coates, R.T., Weglein, A.B., 1996. Internal multiple attenuation using inverse scattering: results from prestack 1 & 2D acoustic and elastic synthetics. In: SEG Technical Program Expanded Abstracts 1996, pp. 1522–1525. https://doi.org/10.1190/1.1826408.
Gu, Z., Wu, R.S., 2021. Internal multiple removal and illumination correction for seismic imaging. IEEE Trans. Geosci. Rem. Sens. 60, 1–11. https://doi.org/10.1109/TGRS.2021.3080210.
Gazdag, J., Sguazzero, P., 1984. Migration of seismic data by phase shift plus interpolation. Geophysics 49, 124–131.
Gu, Z., Geng, J., Wu, R.S., 2023. An application of internal multiple prediction and primary reflection retrieval to salt structures. Geophysics 88 (6), S189–S201. https://doi.org/10.1190/geo2022-0669.1.
Herrmann, F.J., Wang, D., Verschuur, D.J., 2008. Adaptive curvelet-domain primary-multiple separation. Geophysics 73 (3), A17–A21. https://doi.org/10.1190/1.2904986.
Ikelle, L.T., 2006. A construct of internal multiples from surface data only: the concept of virtual seismic events. Geophys. J. Int. 164 (2), 383–393. https://doi.org/10.1111/j.1365-246x.2006.02857.x.
Ikelle, L.T., Erez, I., Yang, X., 2009. Scattering diagrams in seismic imaging: more insights into the construction of virtual events and internal multiples. J. Appl. Geophys. 67 (2), 150–170. https://doi.org/10.1016/j.jappgeo.2008.10.009.
Jakubowicz, H., 1998. Wave equation prediction and removal of interbed multiples. In: SEG Technical Program Expanded Abstracts 1998, pp. 1527–1530. https://doi.org/10.3997/2214-4609.201408173.
Jia, X., Guitton, A., Snieder, R., 2018. A practical implementation of subsalt Marchenko imaging with a Gulf of Mexico data set. Geophysics 83 (5), S409–S419. https://doi.org/10.1190/geo2017-0646.1.
Kosloff, D., Baysal, E, 1983. Migration with the full acoustic equation. Geophysics 48, 677–687.
Li, X., Hu, T.Y., 2009. Surface-related multiple removal with inverse scattering series method. Chin. J. Geophys. 52 (3), 716–724. https://doi.org/10.1002/cjg2.1393.
Li, Z.C., Qu, Y.M., 2022. Research progress on seismic imaging technology. Petrol. Sci. 19 (1), 128–146. https://doi.org/10.1016/j.petsci.2022.01.015.
Liu, Y., Liu, Y., Lu, Q., 2013. Suppression of internal multiples based on virtual events. Glob. Geol. 16 (2), 113–120. https://doi.org/10.3969/j.issn.1673-9736.2013.02.09.
Löer, K., Curtis, A., Meles, G.A., 2016. Relating source-receiver interferometry to an inverse-scattering series to derive a new method to estimate internal multiples. Geophysics 81, Q27–Q40. https://doi.org/10.1190/geo2015-0330.1.
Lomas, A., Curtis, A., 2019. An introduction to Marchenko methods for imaging. Geophysics 84 (2), F35–F45. https://doi.org/10.1190/geo2018-0068.1.
Lomas, A., Curtis, A., 2020. Marchenko methods in a 3-D world. Geophys. J. Int. 220, 296–307. https://doi.org/10.1093/gji/ggz408.
Malcolm, A.E., de Hoop, M.V., 2004. Inverse multiple scattering in the downward-continuation approach. In: SEG Technical Program Expanded Abstracts 2004 Society of Exploration Geophysicists, pp. 1293–1296. https://doi.org/10.1190/1.1851104.
Matson, K., Dragoset, B., 2005. An introduction to this special section Multiple attenuation. Lead. Edge 24, 252. https://doi.org/10.1190/1.1895308.
Meles, G.A., Loer, K., Ravasi, M., Curtis, A., Costa, F.C.A., 2015. Internal multiple prediction and removal using Marchenko autofocusing and seismic interferometry. Geophysics 80 (1), A7–A11. https://doi.org/10.1190/geo2014-0408.1.
Meles, G.A., Wapenaa, K., Curtis, A., 2016. Reconstructing the primary reflections in seismic data by Marchenko redatuming and convolutional interferometry. Geophysics 81 (2), Q15–Q26. https://doi.org/10.1190/geo2015-0377.1.
Neut, J., Vasconcelos, I., Wapenaar, K., 2015. On Green's function retrieval by iterative substitution of the coupled Marchenko equations. Geophys. J. Int. 203, 792–813. https://doi.org/10.1093/gji/ggv330.
Qu, Y., Li, J., Guan, Z., Li, Z., 2020. Viscoacoustic reverse time migration of joint primaries and different-order multiples. Geophysics 85 (2), S71–S87. https://doi.org/10.1190/geo2019-0237.1.
Qu, Y., Huang, C., Liu, C., Li, Z., 2021. Full-path compensated least-squares reverse time migration of joint primaries and different-order multiples for deep-marine environment. IEEE Trans. Geosci. Rem. Sens. 59 (8), 7109–7121. https://doi.org/10.1109/TGRS.2020.3024189.
Ravasi, M., Vasconcelos, I., 2021. An open-source framework for the implementation of large-scale integral operators with flexible, modern high-performance computing solutions: enabling 3D Marchenko imaging by least-squares inversion. Geophysics 86 (5), WC177–WC194. https://doi.org/10.1190/geo2020-0796.1.
Ravasi, M., Vasconcelos, I., Kritski, A., Curtis, A., Filho, C.A.D.C., Meles, G.A., 2016. Target-oriented Marchenko imaging of a north sea field. Geophys. J. Int. 205, 99. https://doi.org/10.1093/gji/ggv528.
Slob, E., Wapenaar, K., 2017. Theory for Marchenko imaging of marine seismic data with free surface multiple elimination. In: 79th Annual International Conference and Exhibition. EAGE, pp. 1–5. https://doi.org/10.3997/2214-4609.201700800.
Slob, E., Wapenaar, K., Broggini, F., Snieder, R., 2014. Seismic reflector imaging using internal multiples with Marchenko-type equations. Geophysics 79 (2), S63–S76. https://doi.org/10.1190/geo2013-0095.1.
Staring, M., Neut, J., Wapenaar, K., 2016. An interferometric interpretation of Marchenko redatuming including free-surface multiples. In: 86th Annual International Meeting, SEG, Expanded Abstracts. https://doi.org/10.1190/segam2016-13956290.1.
Thorbecke, J., Slob, E., Brackenhoff, J., Neut, J., Wapenaar, K., 2017. Implementation of the Marchenko method. Geophysics 82 (6), WB29–WB45. https://doi.org/10.1190/geo2017-0108.1.
Valenciano, A., Chemingui, N., 2015. Introduction to this special section: multiples from attenuation to imaging. Lead. Edge 34, 742. https://doi.org/10.1190/tle34070742.1.
Verschuur, D.J., Berkhout, A.J., Wapenaar, K., 1992. Adaptive surface-related multiple elimination. Geophysics 57 (9), 1166–1177. https://doi.org/10.1190/1.1443330.
Wapenaar, K., Thorbecke, J., Neut, J., Broggini, F., Slob, E., Snieder, R., 2014. Marchenko imaging. Geophysics 79 (3), WA39–WA57. https://doi.org/10.1190/geo2013-0302.1.
Wapenaar, K., de Ridder, S., 2022. On the relation between the propagator matrix and the Marchenko focusing function. Geophysics 87 (2), A7–A11. https://doi.org/10.1190/geo2021-0511.1.
Wapenaar, K., Snieder, R., Ridder, S., Slob, E., 2021. Green's function representations for Marchenko imaging without up/down decomposition. Geophys. J. Int. 227, 184–203. https://doi.org/10.1093/gji/ggab220.
Weglein, A.B., Dragoset, B., 2005. Multiple attenuation. In: SEG, Geophysics Reprint Series. https://doi.org/10.1190/1.9781560801702.ch10.
Weglein, A.B., Gasparotto, F.A., Carvalho, P.M., Stolt, R.H., 1997. An inverse-scattering series method for attenuating multiples in seismic reflection data. Geophysics 62 (6), 1975–1989. https://doi.org/10.1190/1.1444298.
Weglein, A.B., Araújo, F.V., Carvalho, P.M., Stolt, R.H., Matson, K.H., Coates, R.T., Corrigan, D., Foster, D., Shaw, S.A., Zhang, H., 2003. Inverse scattering series and seismic exploration. Inverse Probl. 19 (6), R27. https://doi.org/10.1088/0266-5611/19/6/r01.
Yilmaz, Ö., 2001. Seismic Data Analysis: Processing, Inversion, and Interpretation of Seismic Data. Society of exploration geophysicists. https://doi.org/10.1190/1.9781560801580.fm.
You, J., Cao, J., 2020. Full wave equation depth extrapolation for migration using matrix multiplication. Geophysics 85 (6), S395–S403. https://doi.org/10.1190/geo2019-0323.1.
You, J., Pan, N., Liu, W., Cao, J., 2022. Efficient wavefield separation by reformulation of two-way wave-equation depth-extrapolation scheme. Geophysics 87 (4), S209–S222. https://doi.org/10.1190/geo2021-0629.1.
Zhang, L., Slob, E., 2020. A field data example of Marchenko multiple elimination. Geophysics 85 (2), S65–S70. https://doi.org/10.1190/geo2019-0327.1.
Zhang, L., Slob, E., Wang, Y., Ravasi, M., Kostov, C., 2021. Advances in seismic multiple reflection processing—Introduction. Geophysics 86 (5), WCi–WCii.